CrystEngComm

One Dimensional Halogen Bond Design: Br···N versus I···N with Fluoroarenes

Journal:	*CrystEngComm*
Manuscript ID	CE-ART-06-2021-000864.R1
Article Type:	Paper
Date Submitted by the Author:	26-Jul-2021
Complete List of Authors:	Peloquin, Andrew; United States Air Force Academy, Chemistry; Clemson University, Chemistry McMillen, Colin; Clemson University, Chemistry Pennington, William; Clemson University, Department of Chemistry

SCHOLARONE™
Manuscripts

Please do not adjust margins

ARTICLE

One Dimensional Halogen Bond Design: Br···N versus I···N with Fluoroarenes

Received 00th January 20xx,
Accepted 00th January 20xx

DOI: 10.1039/x0xx00000x

Andrew J. Peloquin, Colin D. McMillen, and William T. Pennington

A series of co-crystallization experiments were performed using 1,4-dibromo- and 1,4-diiodotetrafluorobenzene (Br_2F_4bz and I_2F_4bz), as well as 4,4′-dibromo- and 4,4′-diiodooctafluorobiphenyl (Br_2F_8bph and I_2F_8bph), with nine N-heterocyclic diamines and the bicyclic, tertiary diamine 1,4-diazabicyclo[2.2.2]octane to elucidate trends between benzene and biphenyl-based halogen bond donors, as well as factors influencing the resulting halogen bond strength. The acceptors chosen contain nitrogen atom geometries resulting in the formation of chains and a total of 29 new crystal structures were obtained. In the majority of cases, cocrystals resulting from Br_2F_4bz and I_2F_4bz are isomorphous, as are the structures from Br_2F_8bph and I_2F_8bph, but the observed structures are different for benzene versus biphenyl based derivatives. Analysis of the halogen bond geometries indicates statistically significant correlations between halogen bond distance and both molecular electrostatic potential as well as percent buried volume, a measure of the steric encumbrance of the acceptor nitrogen atoms.

Introduction

Intermolecular interactions lie at the center of understanding most supramolecular and crystal engineering phenomena. While hydrogen bonding is arguably the most well-understood non-covalent interaction, halogen bonding[1] has emerged as an additional tool in solid-state synthesis,[2–4] pharmaceuticals,[5–7] and light-emitting materials.[8–10] The directionality[11] and strength[12] of halogen bonds make them attractive targets for the development and study of crystal engineering synthons.

Iodoperfluoroalkanes and arenes are amongst the most common class of halogen bond donors employed in the engineering of halogen-bonded, crystalline materials. Replacing hydrogen atoms with fluorine atoms increases the positive potential on the halogen bond donor atom and thus increases the strength of the resulting halogen bond.[13–15] One of the most utilized donor molecules of this class is 1,4-diiodotetrafluorobenzene (I_2F_4bz), with 442 crystal structures involving an I···A (A = N, O, S) halogen bond deposited with the Cambridge Structural Database (CSD) to date.[16] However, simple chemical modifications to this archetypal donor molecule result in a precipitous drop in representation in literature. For example, the bromine analog, 1,4-dibromotetrafluorobenzene (Br_2F_4bz) has only 42 crystal structures containing a Br···A (A = N, O, S) deposited to the CSD. Additionally, the biphenyl analogs 4,4′-dibromooctafluorobiphenyl (Br_2F_8bph) and 4,4′-diiodooctafluorobiphenyl (I_2F_8bph) have even less representation in the halogen bonding literature, with only 1 and 11 halogen bonding cocrystals (X···A; X = Br, I; A = N, O, S) respectively deposited to the CSD. The mixed halogen donor, 4-bromo-4′-iodooctafluorobiphenyl has also been occasionally represented in the halogen bonding literature, with 4 structures reported.[17] However, positional disorder of the bromine and iodine atoms complicates the study of its halogen

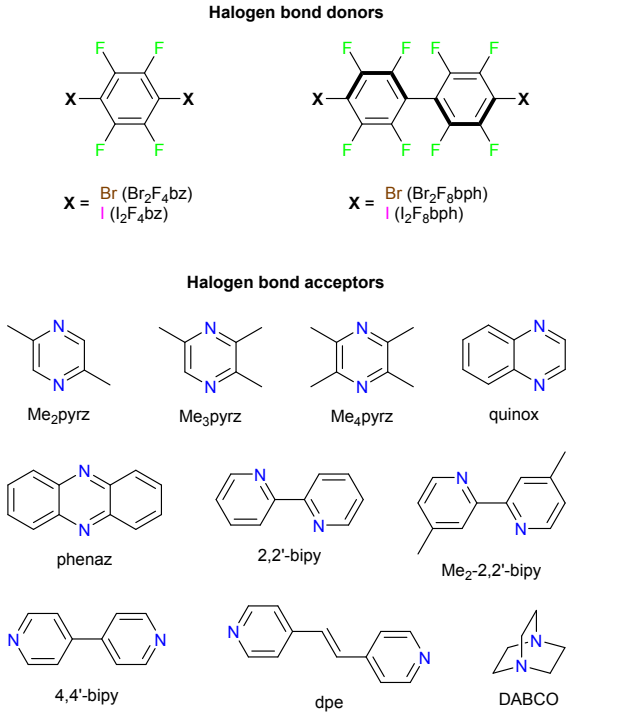

Scheme 1. Scope of halogen bond donors and acceptors utilized in this study

Department of Chemistry, Clemson University, 219 Hunter Laboratories, Clemson, SC 29634-0973, USA. E-mail: billp@clemson.edu
† Electronic Supplementary Information (ESI) available. CCDC reference numbers 2092652–2092661, 2092665–2092673, and 2093037–2093046. For ESI and crystallographic data in CIF or other electronic format see
DOI: 10.1039/x0xx00000x

Please do not adjust margins

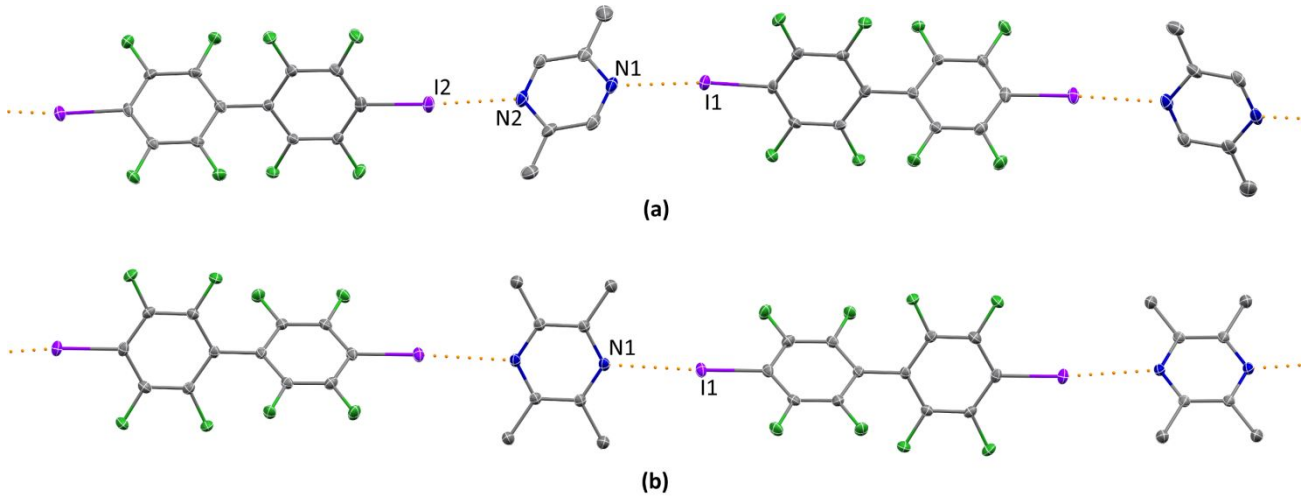

Figure 1. Halogen bonding in (I_2F_8bph)(Me_2pyrz) (a) and (I_2F_8bph)(Me_4pyrz) (b). I···N interactions are shown as orange dotted lines. Hydrogen atoms have been omitted for clarity. Atomic displacement ellipsoids are shown at the 50% probability level.

bonding behavior in terms of systematic comparisons of Br versus I trends.

Given the dearth of literature on these simple, yet relatively unexplored halogen bond donors, this study was designed to isolate halogen bonding cocrystals of similar packing motifs for analysis of the factors influencing halogen bond strength and orientation. Acceptor molecules chosen for this study all contain two nitrogen atoms capable of forming chains in the solid state.

While studies have been presented in the past literature attempting to correlate molecular structure to the resulting cocrystal geometry, they often focus on a single halogen donor molecule[14,18] or contain significant variation in the acceptor.[19] This makes a determination of more general trends difficult. Through rational variation of molecular structure across both multiple halogen bond donors and acceptor molecules in the present study, trends in halogen bond strength versus both electrostatic potential as well the steric environment around the acceptor atom are observed across a large number of cocrystalline structures.

Experimental

Materials

Co-crystals were obtained using commercially available reagents which were used as received, except for I_2F_8bph. This donor was synthesized by a previously published procedure.[20]

Synthesis of cocrystals

The synthesis of all cocrystals was scaled to yield 100 to 150 mg of the desired product. Reagents were dissolved in a minimum amount of ethanol or a 1:1 mixture of dichloromethane:ethanol. The solutions were allowed to evaporate slowly at room temperature. Vials were sealed to halt evaporation as soon as crystals were observed to ensure sample purity. See ESI for full, specific crystal synthesis details.

X-ray structure determination

For single-crystal X-ray analysis, crystals were mounted on low background cryogenic loops using paratone oil. Data were collected using Mo Kα radiation (λ = 0.71073 Å) on either a Bruker D8 Venture diffractometer with an Incoatec Iμs microfocus source and a Photon 2 detector or a Rigaku XtaLAB Synergy diffractometer with a PhotonJet source and a HyPix3000 detector. Diffraction data were collected using ϕ and ω-scans and subsequently processed and scaled using the APEX3 software suite (SAINT/SADABS) or *CrysAlis PRO* 1.171.40.58.[21,22] The structures were solved with the SHELXT structure solution program and refined utilizing *OLEX2*.refine, both incorporated in the *OLEX2* (v1.3) program package.[23–25] All nonhydrogen atoms were refined anisotropically. All hydrogen atoms were placed in geometrically optimized positions using the appropriate riding models. Both the (Br_2F_8bph)(4,4'-bipy) and (I_2F_8bph)(4,4'-bipy) structures were solved as non-merohedral twins. Final refinement was performed against the HKLF4 file, with no significant improvement realized by refinement against the HKLF5. The structure of the (I_2F_8bph)(Me_2pyrz) cocrystal was refined as an inversion twin, with a final BASF of 0.361(17). All geometric parameters within the manuscript body were calculated using *OLEX2*. Selected crystallographic and data collection parameters are listed in Table SI1.

Physical measurements

Thermal analysis was conducted utilizing simultaneous differential scanning calorimetry (DSC) and thermal gravimetric analysis (TGA), carried out under nitrogen, using a TA Instruments Discovery 650. Sample masses ranged from 5–15 mg. Samples were heated from 30°C to 500°C at a rate of 10°C/min. Elemental analyses were performed with a Thermo Elementar Vario EL III combustion analyzer. These results can be found in the ESI.

Quantum theoretical calculations

All calculations were conducted using the Gaussian 09 Rev B.01 package with the ωB897X-D functional and the def2-TZVP

This journal is © The Royal Society of Chemistry 20xx

basis set.[26–28] Molecular electrostatic potential calculations of the acceptor molecules were performed on optimized geometries, and the minimum surface potential was extracted using MultiWFN version 3.7 with an isodensity value of 0.001 a.u.[29]

%V_{bur} calculations

The SambVca 2.0 web application was used to calculate the percent buried volume, %V_{bur}, as a measure of the steric environment around the nitrogen acceptor atoms.[30] The input .pdb files were created using GaussView 6.0 from the previously optimized geometries.[31] For standardization across acceptors, a sphere radius of 4.0 Å and distance of the coordination point from the center of the sphere of 2.85 Å were chosen. Hydrogen atoms were included in the calculation of %V_{bur}.

Results and Discussion

Crystal structure analysis

In an effort to produce cocrystals with a consistent halogen bonding pattern, amines with two opposing nitrogen atoms were chosen as the acceptors of interest. Given the opposing halogen atoms on the donor molecules, we anticipated that 1:1 donor:acceptor cocrystals would likely exhibit one dimensional (1-D) structural features from halogen bonding interactions. Except for the tertiary amine DABCO, all acceptors are based around an aromatic pyrazine or pyridine

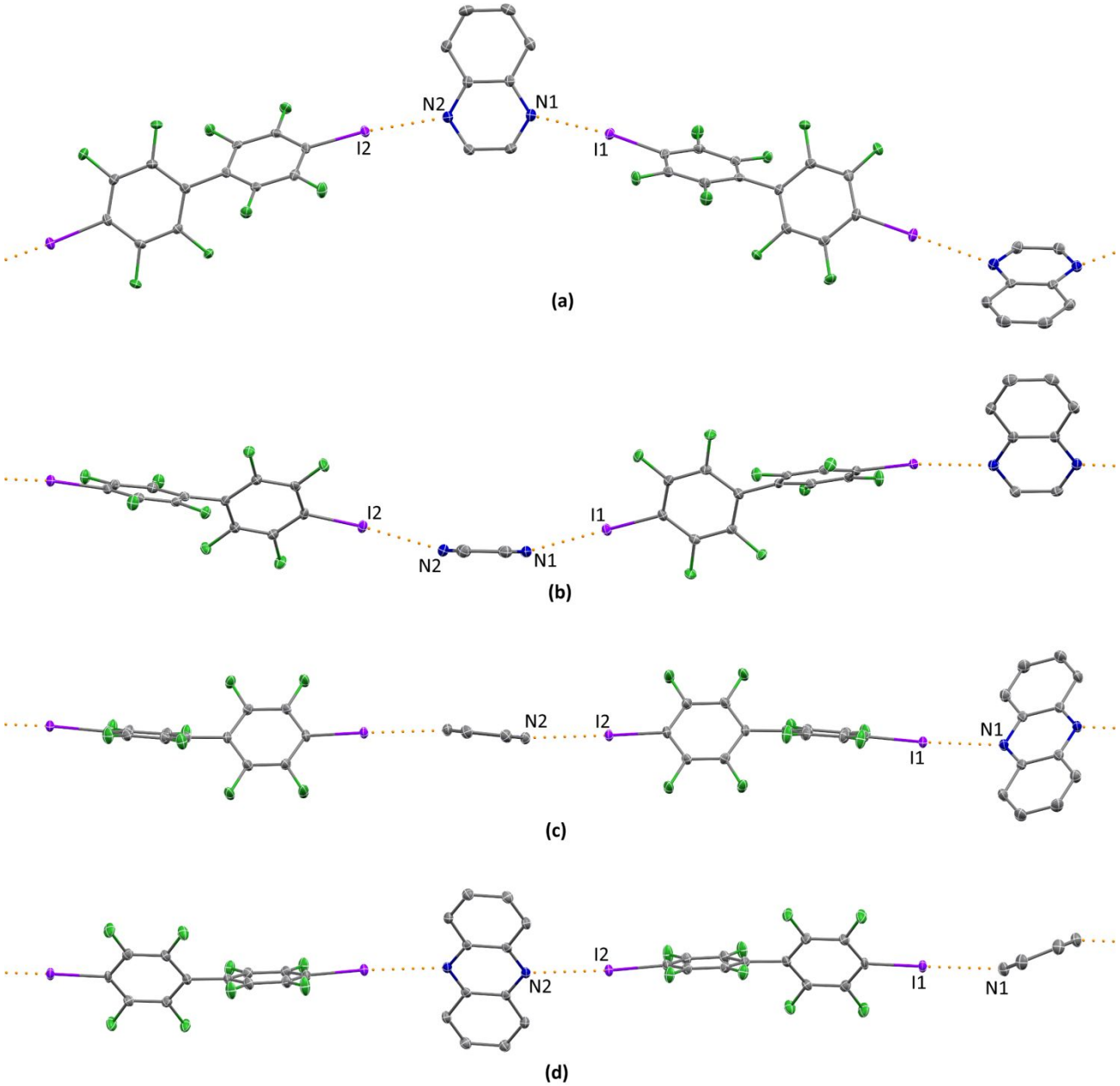

Figure 2. Halogen bonding in (I_2F_8bph)(quinox) (a & b) and (I_2F_8bph)(phenaz) (c & d), highlighting differing orientation of two unique acceptor molecules. I···N interactions are shown as orange dotted lines. Hydrogen atoms have been omitted for clarity. Atomic displacement ellipsoids are shown at the 50% probability level.

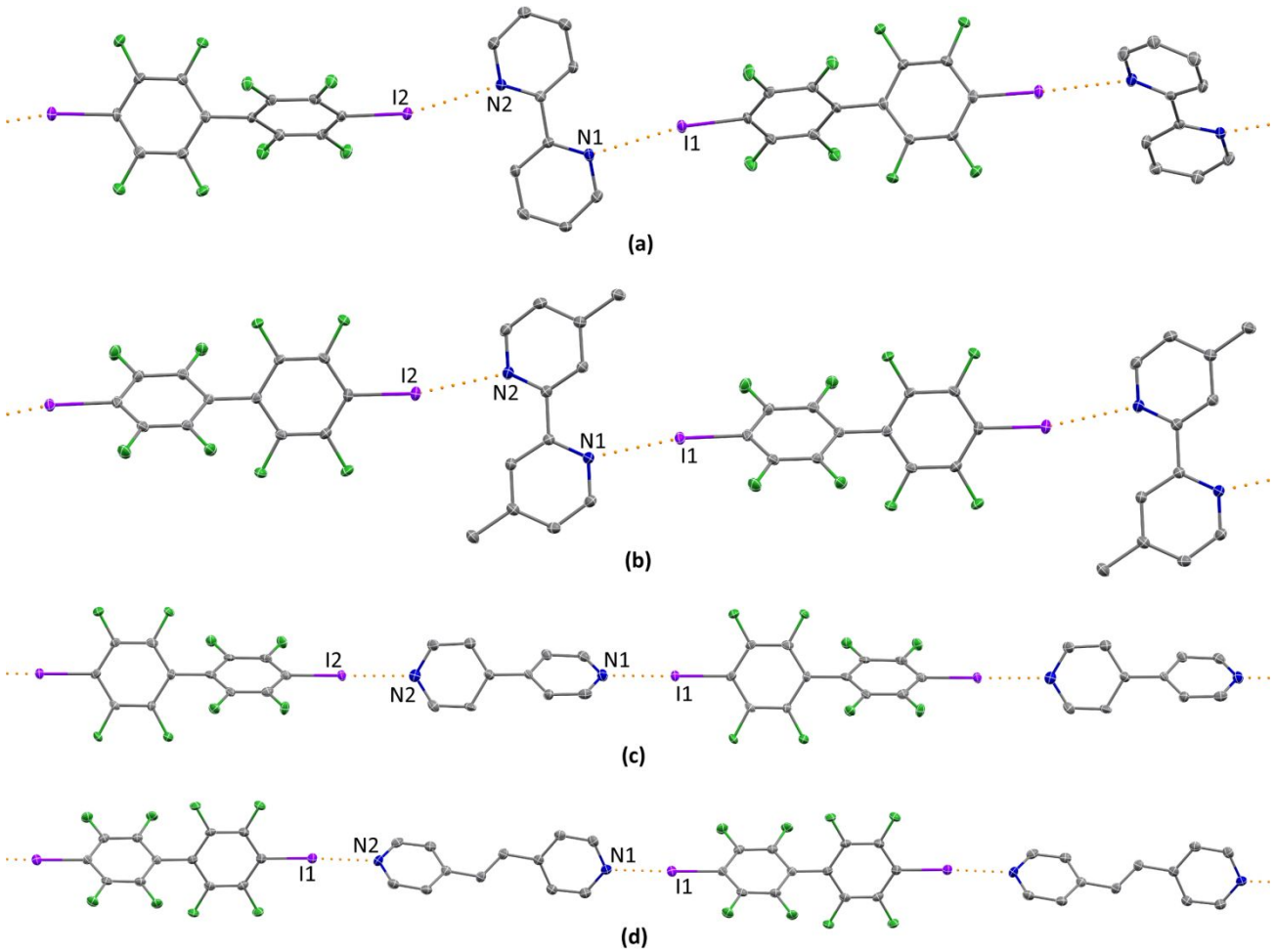

Figure 3. Halogen bonding in (I_2F_8bph)(2,2'-bipy) (a), (I_2F_8bph)(Me_2-2,2'-bipy) (b), (I_2F_8bph)(4,4'-bipy) (c), and (I_2F_8bph)(dpe) (d). I···N interactions are shown as orange dotted lines. Hydrogen atoms have been omitted for clarity. Atomic displacement ellipsoids are shown at the 50% probability level.

core and can be grouped into three categories: the methylated pyrazines 2,5-dimethylpyrazine (Me_2pyrz), 2,3,5-trimethylpyrazine (Me_3pyrz), and 2,3,5,6-tetramethylpyrazine (Me_4pyrz); the polyaromatic pyrazines quinoxaline (quinox) and phenazine (phenaz); and the bipyridine-based acceptors 2,2'-bipyridine (2,2'-bipy), 4,4'-dimethyl-2,2'-bipyridine (Me_2-2,2'-bipy), 4,4'-bipyridine (4,4'-bipy), and 1,2-di(4-pyridyl)ethylene (dpe). Additionally, the bicyclic, tertiary diamine 1,4-diazabicyclo[2.2.2]octane (DABCO) was utilized. When paired with the fluorinated donors Br_2F_4bz, I_2F_4bz, Br_2F_8bph, and I_2F_8bph, which all contain halogen donor atoms in opposing 1,4- or 4,4'-arrangements, 1:1 chains were observed in each cocrystalline structure. In the majority of cases, the X_2F_4bz structures are isomorphous, as are the X_2F_8bph pairs. The two sets form different structure types from one another, leading to a variety of chains that were characterized.

Methylpyrazine acceptors

The series of methylated pyrazines Me_2pyrz, Me_3pyrz, and Me_4pyrz allow for the study of structurally similar acceptors which differ primarily in the degree of methylation proximal to the acceptor nitrogen atoms. For a baseline comparison, the cocrystal of pyrazine and I_2F_4bz has been previously reported, with an I···N distance of 2.934(5) Å (R_{XB} = 0.83).[19] In our hands, all attempts to isolate cocrystalline material of this acceptor with the X_2F_8bph donors were unsuccessful. The symmetrically methylated acceptor 2,5-dimethylpyrazine, which is a liquid at room temperature, provided linear, 1:1 chains with each of the four halogen bond donors (Figure SI28). Despite the steric encumbrance due to the addition of a methyl group adjacent to the acceptor nitrogen atoms, the I···N halogen bond distance is slightly shorter in the (I_2F_4bz)(Me_2pyrz) cocrystal, 2.897(2) Å (R_{XB} = 0.82), than in the aforementioned pyrazine cocrystal. In the X_2F_4bz containing cocrystals, neighboring chains are parallel; however, in the cocrystals with the X_2F_8bph donor, alternating chains are rotated by approximately 30° to one another. The differing orientation of neighboring chains also manifests in a greater degree of segregation of the cocrystal into fluorinated and non-fluorinated regions in the X_2F_4bz-containing cocrystals (Figure SI37-40), which is not significantly observed in the X_2F_8bph-containing structures. The (I_2F_8bph)(Me_2pyrz) cocrystal contains the shortest halogen bond observed within the pyrazine-based acceptor series, 2.881(4) Å (R_{XB} = 0.82), owing at least in part to the increased fluorine:iodine ratio in the biphenyl donor compared to the benzene donor. One cocrystal containing the asymmetrically substituted acceptor Me_3pyrz, (I_2F_4bz)(Me_3pyrz), was obtained (Figure SI41). The I···N halogen bond distance to the α,α'-

This journal is © The Royal Society of Chemistry 20xx

Table 1. Pyridine-pyridine dihedral angles

Bipyridine acceptor	donor	θ (°)
2,2'-bipyridine (2,2'-bipy)	Br_2F_4bz	0.0(4)
	I_2F_4bz	0.0(3)
	Br_2F_8bph	14.46(8)[a]
	I_2F_8bph	13.91(10)
4,4'-dimethyl-2,2'-bipyridine (Me_2-2,2'-bipy)	Br_2F_4bz	0.0(6)
	I_2F_4bz	9.14(15)
	Br_2F_8bph	12.85(4)
	I_2F_8bph	18.90(6)
4,4'-bipyridine (4,4'-bipy)	Br_2F_4bz	0.00(18)
	I_2F_4bz	0.0(2)
	Br_2F_8bph	52.6(3)
	I_2F_8bph	54.0(2)
1,2-di(4-pyridyl)ethylene (dpe)	Br_2F_4bz	0.0(2)
	I_2F_4bz	0.0(2)
	Br_2F_8bph	34.29(10)
	I_2F_8bph	59.64(12)

a In the solid-state structure of (Br_2F_8bph)(2,2'-bipy), three unique 2,2'-bipy molecules are present. Two are planar. The dihedral of the third is tabulated.

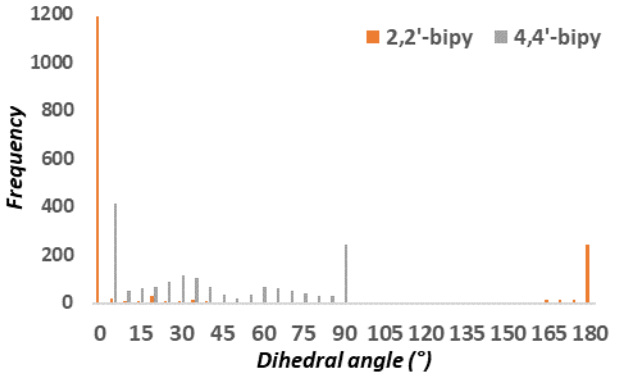

Figure 4. Frequency plot of 2,2'-bipyridine and 4,4'-bipyridine ring dihedral angles as deposited in CSD. For 2,2'-bipyridine, the dihedral angle is defined to include both nitrogen atoms. Metal-containing structures have been omitted to remove the influence of bidentate coordination. The symmetry of 4,4'-bipyridine limits dihedral angles to the range of 0° to 90°.

dimethylated nitrogen atom is longer, 3.007(4) Å (R_{XB} = 0.85), than to the α-methylated nitrogen atom, 2.909(4) Å (R_{XB} = 0.82). The N···I distance to the α,α'-dimethylated nitrogen atom is comparable to that in the previously reported (I_2F_4bz)(Me4pyrz) cocrystal (3.0665(18) Å, R_{XB} = 0.87).[32] Finally, the fully methylated acceptor Me_4pyrz produces 1:1 parallel chains with three of the donors, with Br_2F_4bz producing (Br_2F_4bz)(Me_4pyrz)$_2$ cocrystals (Figure SI29). In the 1:1 cases, the overall packing is remarkably similar in each case. The I···N distances are approximately 0.1 Å longer as compared to the Me_2pyrz distances, a consequence of the increased steric encumbrance of the additional methylation. For example, the shortest I···N distance in (I_2F_8bph)(Me_2pyrz) is 2.881(4) Å (R_{XB} = 0.82), which is lengthened to 3.0187(19) Å (R_{XB} = 0.86).

Polyaromatic pyrazine acceptors

In contrast to the methyl pyrazine-containing cocrystals, the cocrystals obtained utilizing the polyaromatic acceptor quinoxaline and phenazine do not produce linear halogen bonded chains (Figure 2). The acceptor quinoxaline produces cocrystals with all four donors showing significant corrugation (Figure SI30).[33] This deviation is attributed to the asymmetry of the quinoxaline molecule, as the halogen bonds deviate away from the phenyl portion of the acceptor. With phenazine, the donors Br_2F_4bz and I_2F_4bz do not produce halogen bonding chains at all, with the second nitrogen atom involved instead in a hydrogen bonding interaction to another phenazine molecule.[34] However, with the biphenyl donors, the symmetry of phenazine again results in the formation of 1-D halogen bonding chains (Figure SI31). Each unique phenazine molecule in the chain is inclined to a varying degree relative to the direction of chain propagation, resulting in small kinks in the chain. As the inclination of the phenazine plane does not significantly disturb the I···N···N···I coplanarity, the overall linearity of the chain is far less perturbed than with quinoxaline.

Bipyridine acceptors

Cocrystals involving the bipyridine-based acceptors 2,2'-bipyridine, 4,4'-dimethyl-2,2'-bipyridine, 4,4'-bipyridine, and 1,2-di(4-pyridyl)ethylene, again exhibit 1-D halogen bonded motifs (Figures SI33–SI36). Chains involving nitrogen atoms at the 4-positions are generally straight since the nitrogen atoms directly oppose one another (Figure 3, c-d). When the nitrogen atoms are in the 2-positions, a small step is introduced in the chain (Figure 3, a-b). In the bipyridine series, two notable trends are observed. First, the halogen bond distance is reduced with reduced steric encumbrance around the acceptor nitrogen atom. For example, with 4,4'-bipyridine, the shortest I···N distance with I_2F_8bph is 2.734(6) Å, but this interaction distance elongates with 2,2'-bipyridine, with the longest measured at 3.091(2) Å. A second trend is observed with the geometry of the acceptor molecules. In cocrystals utilizing the X_2F_4bz donors, the pyridine ring planes are coplanar (or parallel, but not coplanar in the case of 1,2-di(4-pyridyl)ethylene due to the presence of the ethylene linker). When the X_2F_8bph donors are employed, a significant ring-to-ring dihedral angle is observed. The most extreme case of this rotation occurs in (I_2F_8bph)(dpe) where the angle between pyridine planes is 59.64(12)°. The observed intermediate rotation of the pyridine planes is uncommon. For 2,2'-bipyridine, 92% of organic-only structures have dihedral angles within 5° or coplanar or orthogonal. While the solid-state structures of a given acceptor with Br_2F_8bph and I_2F_8bph are isomorphous in the majority of cases presented in this study, a comparison of the dihedral angles reveals that the bipyridine-based acceptors do not follow this trend. In the case of 2,2'-bipyridine, three distinct acceptor molecules are present with Br_2F_8bph (one whole and two half molecules in the asymmetric unit), whereas only a single acceptor is present in the structure with I_2F_8bph. The overall packing still involves the formation of chains in both cases, but the relative positioning of neighboring chains varies between the two (Figure SI32). With 1,2-di(4-pyridyl)ethylene, chains are again formed in both

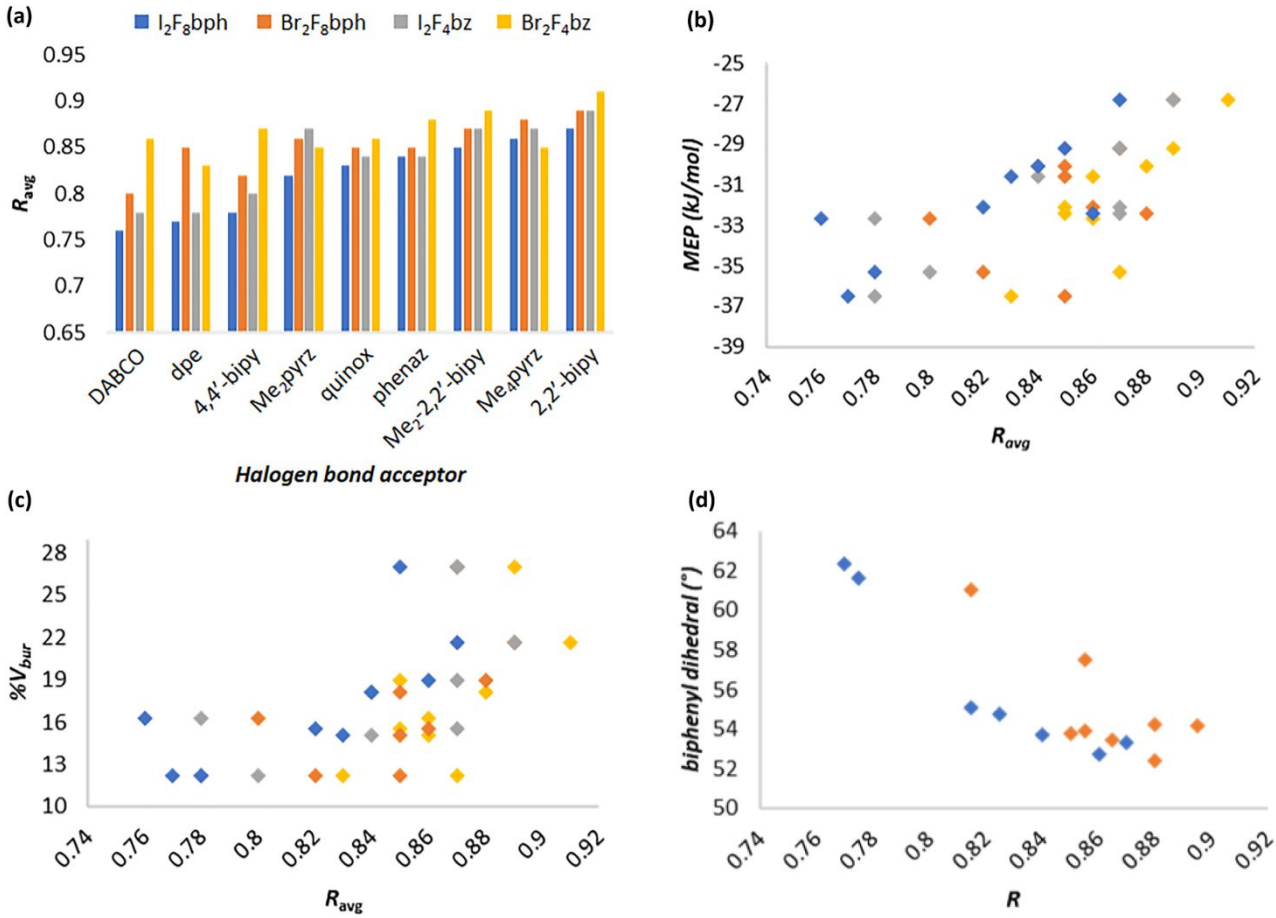

Figure 5. Graphical representation of R_{avg} compared to halogen bond acceptor (a), MEP (b), $\%V_{bur}$ (c), and biphenyl dihedral angle (d). Data is color-coded by halogen bond donor, with colors noted above a.

cases, with the relative positioning of neighboring chains being different (Figure SI35). Another notable exception to the X_2F_4bz/X_2F_8bph grouping of bipyridine dihedral angles occurs with 4,4'-Me_2-2,2'-bipy. With this acceptor, the bipyridine dihedral angle gradually increases from coplanar (0.0(6)°) with Br_2F_4bz to 18.90(6)° with I_2F_8bph. The remaining two donors are intermediate, as opposed to grouping with their aromatic scaffold partner. An additional dpe containing cocrystal was also identified, $(Br_2F_8bph)_2$(dpe). In this case, chains are formed through the combination of a Br···N halogen bond to one end of the biphenyl donor, with the other ends linking through a weak type I Br···Br contact (3.6542(2) Å, R_{XB} = 0.99)

DABCO as an acceptor

Finally, the cocrystals of Br_2F_8bph and I_2F_8bph with 1,4-diazabicyclo[2.2.2]octane (DABCO) were obtained (Figure SI36). In contrast to the previously reported Br_2F_4bz and I_2F_4bz cocrystals with DABCO,[34] which are not isomorphous, the (Br_2F_8bph)(DABCO) and (I_2F_8bph)(DABCO) cocrystals are. Both cocrystals of the biphenyl donors form chains with a modest undulation to the chain, which more closely resembles the chains of (Br_2F_4bz)(DABCO), versus those of (I_2F_4bz)(DABCO) in which the chains are nearly perfectly linear. With an I···N distance of 2.6652(19) Å (R_{XB} = 0.76), the (I_2F_8bph)(DABCO) cocrystal contains the shortest halogen bond present in this study. This is again slightly shorter than the analogous (I_2F_4bz)(DABCO) cocrystal, with an I···N distance of 2.7350(8) Å (R_{XB} = 0.77). Also isolated during attempts at obtaining the 1:1 cocrystal was $(Br_2F_8bph)_2$(DABCO) (Figure SI62). At this ratio, chain formation is interrupted, and instead discrete $(Br_2F_8bph)_2$(DABCO) units are observed, with only one bromine atom of each donor molecule participating in a halogen bond. The second bromine atoms of two biphenyl molecules do approach one another but at a distance equal to the sum of van der Waals radii.

Structural correlations

Given the large amount of structural data provided within this report, in addition to the related structures in the literature (Table SI2), several noteworthy trends can be elucidated. In all cases, the measured I···N distances in cocrystals of a particular acceptor are shorter with I_2F_8bph than I_2F_4bz, likely due to the increased fluorine:iodine ratio of the biphenyl-based donor relative to the benzene-based donor (Figure 5a). The same trend holds in most cases for the Br_2F_8bph and Br_2F_4bz donor series, with the Me_2pyrz, Me_4pyrz, and dpe acceptors as exceptions. For these acceptors, the Br···N distances are slightly asymmetric for the Br_2F_8bph cocrystals, while the distances in the Br_2F_4bz cocrystals are symmetric, which may skew this particular analysis. This difference in halogen bond

This journal is © The Royal Society of Chemistry 20xx

Please do not adjust margins

Table 2. Molecular electrostatic potential (MEP) for halogen bond acceptors and donors, and percent buried volume (%V_{bur}) for halogen bond acceptors

acceptor	MEP (kJ/mol)	%V_{bur}
2,5-dimethylpyrazine (Me_2pyrz)	-32.1	15.5
2,3,5-trimethylpyrazine (Me_3pyrz)	-33.5 [a]	18.3
	-32.0	15.0
2,3,5,6-tetramethylpyrazine (Me_4pyrz)	-32.4	19.0
quinoxaline (quinox)	-30.6	15.1
phenazine (phenaz)	-30.1	18.1
2,2′-bipyridine (2,2′-bipy)	-26.8	21.6
4,4′-dimethyl-2,2′-bipyridine (Me_2-2,2′-bipy)	-29.2	27.0
4,4′-bipyridine (4,4′-bipy)	-35.3	12.2
1,2-di(4-pyridyl)ethylene (dpe)	-36.5	12.2
1,4-diazabicyclo[2.2.2]octane (DABCO)	-32.7	16.3
1,4-dibromotetrafluorobenzene (Br_2F_4bz)	24.4	–
1,4-diiodotetrafluorobenzene (I_2F_4bz)	32.6	–
4,4′-dibromooctafluorobiphenyl (Br_2F_8bph)	25.0	–
4,4′-diiodooctafluorobiphenyl (I_2F_8bph)	33.3	–

a For the asymmetrically methylated acceptor Me_3pyrz, the first row corresponds to the α,α′ disubstituted nitrogen atom

strength contributes to increased melting temperatures of the I_2F_8bph cocrystals relative to their Br_2F_8bph analogs. The two acceptors for which all four XB donor structures are newly reported here, Me_2pyrz (Figure SI1–SI4) and Me_2-2,2′-bipy (Figure SI17-SI20), further support this trend. In both cases, the melting point of the I_2F_4bz cocrystal is higher than that of the Br_2F_4bz one, and the I_2F_8bph cocrystals melt at a higher temperature than that of the X_2F_4bz cocrystals. When Me_2-2,2′-bipy acts as the XB acceptor, the Br_2F_8bph cocrystal melts at approximately the same temperature as the I_2F_8bph cocrystal (140°C and 137°C). Due to the previously described variation in structure with this donor, this deviation from the general trend is unsurprising.

Amongst the cocrystals containing a biphenyl-based donor and a heteroaromatic acceptor, a statistically significant correlation between increased phenyl-phenyl dihedral angle and increasing halogen bond strength (decreasing R_{XB}) is observed (p = 0.043 for Br_2F_8bph and p = 0.0133 for I_2F_8bph) (Figure 5d). A previous computation study has shown strong electron donors to decrease the biphenyl torsion angle.[35] A halogen bond approaches this effect in reverse, with a strong halogen bond (smaller R_{XB}) allowing a larger extent of electron donation away from the pyridine nitrogen atom and out of the π system, thereby allowing a larger dihedral angle. As previously described, the Me_2-2,2′-bipy systems show a dissimilar grouping of structural motifs compared to the other systems of study. The significantly larger %V_{bur} may necessitate subtle packing differences between the organoiodine and organobromine congeners and may further manifest in an increased dihedral angle relative to the other acceptors, and as such, these cocrystals do not fit this particular trend. Regression analysis further supports their consideration as outliers (standardized residual of 4.55 for (I_2F_8bph)(Me_2-2,2′-bipy) and 3.37 for (Br_2F_8bph)(Me_2-2,2′-bipy).

Molecular electrostatic potential (MEP) has often been utilized to described trends in halogen bonding, as well as other intermolecular interactions, although exceptions to the utility of this measure have also been pointed out in the literature.[36–39] For this particular series of halogen bond donors and acceptors, a statistically signific correlation was observed between MEP and X···N distance for Br_2F_4bz (p = 0.0062), I_2F_4bz (p = 0.0135), and I_2F_8bph (p = 0.0095), while the correlation is not significant for Br_2F_8bph (p = 0.1146) (Figure 5b).

While some observational correlation between steric encumbrance and halogen bond distance has been discussed, for example in Me_2pyrz and Me_4pyrz cocrystals, this correlation holds across the entire series of acceptors as well. To quantify the steric encumbrance of each halogen bond acceptor, percent buried volume (%V_{bur}) was utilized. This measure is a common tool for analyzing the binding geometries of ligands in coordination chemistry.[40–42] Analysis indicates a significant correlation between %V_{bur} and X···N distance for for Br_2F_4bz (p = 0.0426), I_2F_4bz (p = 0.0419), and I_2F_8bph (p = 0.0317), while the correlation is again not significant for Br_2F_8bph (p = 0.1131) (Figure 5c). As has been noted, the Br_2F_8bph containing cocrystals often have asymmetric Br···N distances or multiple unique donor:acceptor pairs within the structure, which likely contributes to the lack of statistical significance in the trends for this donor. The varied results of this trend analysis point to the complexity of crystal packing and the difficultly of pointing to a singular, specific factor in attempts to correlate molecular structure and intermolecular interactions in the solid state.

Conclusions

In summary, we have demonstrated the successful cocrystallization of 4,4′-dibromooctafluorobiphenyl and 4,4′-diiodooctafluorobiphenyl, the biphenyl analogs to the common 1,4-dibromobenzene and 1,4-diiodobenzene halogen bond donors, with a series of difunctional halogen bond acceptors. The 1:1 cocrystals of these donors and acceptors favor the formation of 1-D structural motifs via halogen bonding. In the majority of cases, the cocrystals of diiodo- and dibromo- donors with each acceptor molecule are isomorphous with one another for a given donor X2F8bph or X2F4bz donor, though some subtleties in crystal packing led to occasional deviations. The extensive series of structures obtained having 1-D motifs enabled a statistical analysis of various factors influencing the halogen bond strength. In general, for a given acceptor, the iodine-based donors exhibited stronger halogen bonding (in terms of the normalized halogen bond length R_{XB}) than their bromine-based congeners. In this regard, the increased fluorine content of the X_2F_8bph donors compared to the X_2F_4bz donors also contributed to stronger halogen bonds. The molecular electrostatic potential and percent buried volume descriptors exhibited statistically significant correlations to halogen bond distance for three of the four donor molecules present in the study (with Br_2F_8bph not showing a significant correlation). Additionally, a significant correlation was observed between the biphenyl dihedral angle in both biphenyl donors versus the

Please do not adjust margins

accompanying halogen bond length with the aromatic acceptors. These results significantly expand the available structural data for these particular halogen bond donors, while at the same time allowing for the description of statistically significant correlations between molecular structure and the resulting crystal packing.

Conflicts of interest

There are no conflicts to declare.

Acknowledgements

AJP acknowledges the United States Air Force Institute of Technology Civilian Institutions program and the Air Force Office of Scientific Research for fellowship support. We also acknowledge Clemson University for the generous allotment of computational time on the Palmetto cluster.

Notes and references

1 G. R. Desiraju, P. Shing Ho, L. Kloo, A. C. Legon, R. Marquardt, P. Metrangolo, P. Politzer, G. Resnati and K. Rissanen, *Pure Appl. Chem.*, 2013, **85**, 1711–1713.
2 A. Abate, M. Brischetto, G. Cavallo, M. Lahtinen, P. Metrangolo, T. Pilati, S. Radice, G. Resnati, K. Rissanen and G. Terraneo, *Chem. Commun.*, 2010, **46**, 2724–2726.
3 K. Raatikainen, J. Huuskonen, M. Lahtinen, P. Metrangolo and K. Rissanen, *Chem. Commun.*, 2009, 2160–2162.
4 P. Metrangolo, Y. Carcenac, M. Lahtinen, T. Pilati, K. Rissanen, A. Vij and G. Resnati, *Science (80-.).*, 2009, **323**, 1461–1464.
5 Y. Lu, T. Shi, Y. Wang, H. Yang, X. Yan, X. Luo, H. Jiang and W. Zhu, *J. Med. Chem.*, 2009, **52**, 2854–2862.
6 A. A. Bhattacharya, S. Curry and N. P. Franks, *J. Biol. Chem.*, 2000, **275**, 38731–38738.
7 S. W. Rowlinson, J. R. Kiefer, J. J. Prusakiewicz, J. L. Pawlitz, K. R. Kozak, A. S. Kalgutkar, W. C. Stallings, R. G. Kurumbail and L. J. Marnett, *J. Biol. Chem.*, 2003, **278**, 45763–45769.
8 C. L. Sun, J. Li, H. W. Geng, H. Li, Y. Ai, Q. Wang, S. L. Pan and H. L. Zhang, *Chem. - An Asian J.*, 2013, **8**, 3091–3100.
9 D. Yan, A. Delori, G. O. Lloyd, T. Friščić, G. M. Day, W. Jones, J. Lu, M. Wei, D. G. Evans and X. Duan, *Angew. Chemie - Int. Ed.*, 2011, **50**, 12483–12486.
10 D. Yan, D. K. Bučar, A. Delori, B. Patel, G. O. Lloyd, W. Jones and X. Duan, *Chem. - A Eur. J.*, 2013, **19**, 8213–8219.
11 P. Politzer, J. S. Murray and T. Clark, *Phys. Chem. Chem. Phys.*, 2010, **12**, 7748–7757.
12 M. Kolář, J. Hostaš and P. Hobza, *Phys. Chem. Chem. Phys.*, 2014, **16**, 9987–9996.
13 C. Präsang, A. C. Whitwood and D. W. Bruce, *Cryst. Growth Des.*, 2009, **9**, 5319–5326.
14 A. De Santis, A. Forni, R. Liantonio, P. Metrangolo, T. Pilati and G. Resnati, *Chem. - A Eur. J.*, 2003, **9**, 3974–3983.
15 R. B. Walsh, C. W. Padgett, P. Metrangolo, G. Resnati, T. W. Hanks and W. T. Pennington, , DOI:10.1021/cg005540m.
16 C. R. Groom, I. J. Bruno, M. P. Lightfoot and S. C. Ward, *Acta Crystallogr. Sect. B Struct. Sci. Cryst. Eng. Mater.*, 2016, **72**, 171–179.
17 C. B. Aakeroy, P. D. Chopade and J. Desper, *Cryst. Growth Des.*, 2013, **13**, 4145–4150.
18 A. Forni, *J. Phys. Chem. A*, 2009, **113**, 3403–3412.
19 N. Bedeković, V. Stilinović, T. Friščić and D. Cinčić, *New J. Chem.*, 2018, **42**, 10584–10591.
20 A. V. Rozhkov, A. A. Eliseeva, S. V. Baykov, B. Galmés, A. Frontera and V. Y. Kukushkin, *Cryst. Growth Des.*, 2020, **20**, 5908–5921.
21 Bruker. APEX3. Bruker AXS: Madison, WI, USA 2015.
22 Rigaku, OD. CrysAlis PRO. Rigaku Oxford Diffraction Ltd, Yarnton, England, 2018.
23 G. M. Sheldrick, *Acta Crystallogr. Sect. C Struct. Chem.*, 2015, **71**, 3–8.
24 O. V. Dolomanov, L. J. Bourhis, R. J. Gildea, J. A. K. Howard and H. Puschmann, *J. Appl. Crystallogr.*, 2009, **42**, 339–341.
25 L. J. Bourhis, O. V. Dolomanov, R. J. Gildea, J. A. K. Howard and H. Puschmann, *Acta Crystallogr. Sect. A*, 2015, **71**, 59–75.
26 M. J. Frisch, G. W. Trucks, H. B. Schlegel, G. E. Scuseria, M. A. Robb, J. R. Cheeseman, G. Scalmani, V. Barone, B. Mennucci, G. A. Petersson, H. Nakatsuji, M. Caricato, X. Li, H. P. Hratchian, A. F. Izmaylov, J. Bloino, G. Zheng, J. L. Sonnenberg, M. Hada, M. Ehara, K. Toyota, R. Fukuda, J. Hasegawa, M. Ishida, T. Nakajima, Y. Honda, O. Kitao, H. Nakai, T. Vreven, J. A. Montgomery, Jr., J. E. Peralta, F. Ogliaro, M. Bearpark, J. J. Heyd, E. Brothers, K. N. Kudin, V. N. Staroverov, T. Keith, R. Kobayashi, J. Normand, K. Raghavachari, A. Rendell, J. C. Burant, S. S. Iyengar, J. Tomasi, M. Cossi, N. Rega, J. M. Millam, M. Klene, J. E. Knox, J. B. Cross, V. Bakken, C. Adamo, J. Jaramillo, R. Gomperts, R. E. Stratmann, O. Yazyev, A. J. Austin, R. Cammi, C. Pomelli, J. W. Ochterski, R. L. Martin, K. Morokuma, V. G. Zakrzewski, G. A. Voth, P. Salvador, J. J. Dannenberg, S. Dapprich, A. D. Daniels, O. Farkas, J. B. Foresman, J. V. Ortiz, J. Cioslowski, and D. J. Fox, Gaussian 09 B.01, Gaussian, Inc., Wallingford CT, 2010.
27 F. Weigend, *Phys. Chem. Chem. Phys.*, 2006, **8**, 1057–1065.
28 F. Weigend and R. Ahlrichs, *Phys. Chem. Chem. Phys.*, 2005, **7**, 3297–3305.
29 T. Lu and F. Chen, *J. Comput. Chem.*, 2012, **33**, 580–592.
30 L. Falivene, Z. Cao, A. Petta, L. Serra, A. Poater, R. Oliva, V. Scarano and L. Cavallo, *Nat. Chem.*, 2019, **11**, 872–879.
31 R. Dennington, T. A. Keith, and J. M. Millam. GaussView, Version 6, Semichem Inc., Shawnee Mission, KS, 2016.
32 J. L. Syssa-Magale, K. Boubekeur, P. Palvadeau, A. Meerschaut and B. Schöllhorn, *CrystEngComm*, 2005, **7**, 302–308.
33 N. Bedeković, V. Stilinović, T. Friščić and D. Cinčić, *New J. Chem.*, 2018, **42**, 10584–10591.
34 D. Cinčić, T. Friščič and W. D. Jones, *Chem. Mater.*, 2008, **20**, 6623–6626.
35 M. Gõmez-Gallego, M. Martín-Ortiz and M. A. Sierra, *European J. Org. Chem.*, 2011, 6502–6506.

This journal is © The Royal Society of Chemistry 20xx

36 S. M. Huber, E. Jimenez-Izal, J. M. Ugalde and I. Infante, *Chem. Commun.*, 2012, **48**, 7708–7710.
37 V. Oliveira, E. Kraka and D. Cremer, *Phys. Chem. Chem. Phys.*, 2016, **18**, 65–74.
38 J. Thirman, E. Engelage, S. M. Huber and M. Head-Gordon, *Phys. Chem. Chem. Phys.*, 2018, **20**, 905–915.
39 J. M. Holthoff, E. Engelage, R. Weiss and S. M. Huber, *Angew. Chemie - Int. Ed.*, 2020, **59**, 11150–11157.
40 H. Clavier and S. P. Nolan, *Chem. Commun.*, 2010, **46**, 841–861.
41 L. Falivene, R. Credendino, A. Poater, A. Petta, L. Serra, R. Oliva, V. Scarano and L. Cavallo, *Organometallics*, 2016, **35**, 2286–2293.
42 A. Gómez-Suárez, D. J. Nelson and S. P. Nolan, *Chem. Commun.*, 2017, **53**, 2650–2660.

This journal is © The Royal Society of Chemistry 20xx